analytical chemistry

pubs.acs.org/ac
Article

A Live Bacterial Screening Assay for Membrane-Active Antimicrobial Compounds Using Imaging Fluorescence Correlation Spectroscopy

Shiwen Zhu, Yu Wang, Shi Min Sherilyn Chong, and Thorsten Wohland*

Cite This: Anal. Chem. 2025, 97, 9648−9654
Read Online

ABSTRACT: There is a growing need in the personal hygiene industry to develop a new generation of effective antimicrobial actives, to be used as functional antibacterial ingredients and preservatives. Antimicrobials that attack bacterial membranes are an attractive target due to the relatively conserved structure compositions of the bacterial membrane, which bacteria cannot easily change without influences on the function of membrane-embedded proteins. However, current screening is slow and there is a demand for rapid screening methodologies to overcome the time-consuming nature of existing screening tools. Imaging total internal reflection-fluorescence correlation spectroscopy (ITIR-FCS) is a powerful technique that can measure membrane dynamics and identify changes with high accuracy and precision. We therefore combine ITIR-FCS with a segmentation algorithm to automatically identify bacterial cells to screen the effect of antimicrobial compounds on the dynamics of bacterial membranes as a function of antimicrobial concentration and incubation time. This allows to assess membrane activity within less than 30 min and generates dose−response curves within a span of 2 h. The technique detects antimicrobial activity at lower concentrations and an order of magnitude faster than commonly used susceptibility testing assays.

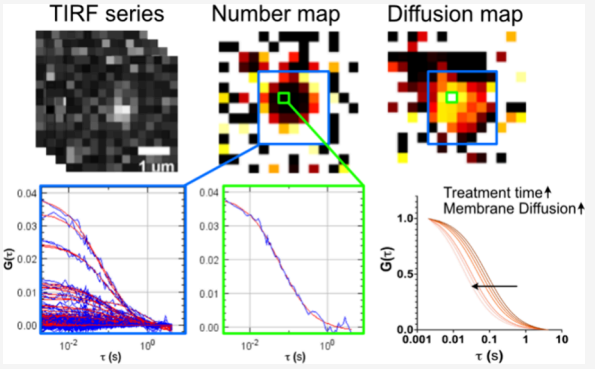

The importance of developing effective preservatives and antimicrobial actives cannot be overstated, as they play a crucial role in extending the shelf life of products, safeguarding public health, and minimizing microbial contamination that threatens human wellbeing.[1,2] With the rising concerns surrounding synthetic preservatives and their potential adverse effects, there is a pressing need for innovative, environmental-friendly, and effective alternatives. One strategy to avoid the development of bacterial resistance against antimicrobials is the targeting of the bacterial envelope.[3] This provides pathogen specificity due to the distinctive structure and composition of the bacterial membranes.[4] It is challenging for bacteria to modify their membrane, given that alternations could impact the functionality of the embedded proteins.[5−8] Hence, the lipid dynamics of the membrane is an important indicator of bacterial health and integrity which can provide meaningful information on the membrane status. However, lipid diffusion on live bacterial cell membranes has been seldomly documented to date due to their small size.[9−11]

Besides commonly used susceptibility testing, including gradient method and disk diffusion test, new techniques have been deployed for screening bacteria libraries such as microfluidics[12,13] and mass spectrometry.[14,15] Despite advancements, these techniques remain constrained in their scope, are time-intensive, and are susceptible to errors. Thus, there is a need for a time-efficient and quantitative screening tool.

Imaging Fluorescence Correlation Spectroscopy (Imaging FCS)[16−18] is a technique that records and statistically analyzes the fluorescence fluctuations at each pixel of an image time series. The fluorescence fluctuations provide information on the underlying dynamics of the sample if the data is acquired sufficiently fast, i.e. about ten times faster than the process to be measured. Imaging FCS has been implemented in total internal reflection (TIR),[19−21] variable angle illumination (VAI)[22] or single plane illumination microscopes (SPIM).[17,23] Here we employ Imaging Total Internal Reflection-Fluorescence Correlation Spectroscopy (ITIR-FCS) to monitor the dynamics of basal membranes of fluorescently labeled bacterial cells attached to a coverslip. ITIR-FCS is ideal for this task as it generates high-contrast fluorescence images with minimal background and virtually no out-of-focus light.

Using ITIR-FCS we record 50,000 frames at 2 ms per frame to analyze the diffusion of membrane stains in live bacteria. We perform these measurements at regular intervals to track

Received: October 23, 2024
Revised: April 1, 2025
Accepted: April 2, 2025
Published: April 30, 2025

https://doi.org/10.1021/acs.analchem.4c05698
Anal. Chem. 2025, 97, 9648−9654

changes of bacterial membrane dynamics in relation to both, antimicrobial concentration and time after addition. This procedure allows us to evaluate membrane behavior in under half an hour and construct dose−response curves within a time frame of 1−2 h. The method was applied to *Staphylococcus aureus* (*S. aureus*), and demonstrated that antimicrobials disturb the lipid membrane at subminimum inhibitory concentration (MIC) by altering lipid diffusivity in a dose- and time-dependent manner.

As a comparison we used Isothermal microcalorimetry (IMC), which has been widely employed in microbiology as it is able to measure heat produced in the microwatt range under isothermal conditions.[24] As living microbial cells produce heat during growth, IMC can be used to measure microbial metabolic activity.[25,26]

Prior work by von Ah et al. (2009)[27] has categorized several Mechanism of Action (MoA) of known antibiotics into cell wall synthesis inhibitors, protein synthesis inhibitors, and DNA synthesis inhibitors, using heat flow profiles.[27] These results suggest the prospects of using IMC for antimicrobial agents at subinhibitory concentrations.

Here we leverage IMC to investigate the antimicrobial mechanism of representative preservative compounds to cross-validate with ITIR-FCS method. Our results show that ITIR-FCS is superior in sensitivity and response time to detect antimicrobial-induced changes in membrane dynamics compared to traditional industry screening methods.

MATERIALS AND METHODS

***S. aureus* Growth Kinetics.** *Growth Curve Analysis and MIC Assay.* The growth curve analysis of *Staphylococcus aureus* ATCC 6538 (ATCC, VA, USA) in the presence of each antimicrobial compound was carried out using the broth microdilution method. Clear 96-well flat-bottom Costar cell culture plates (Corning, NY, USA) were filled with 100 μL of Tryptic Soy Broth (TSB, Becton Dickinson, Singapore), in each well. AN antimicrobial compound was added to the first well in each row to create two times the desired highest working concentration. Subsequently, a 2-fold serial dilution was carried out starting from the first well in each row. Overnight culture of either *S. aureus* was adjusted to ∼ 5 Log10 Colony Forming Unit (CFU) /ml. A volume of 100 μL of the adjusted culture was added to each well. The plates were incubated at 37 °C in the Infinite 200 Pro (Tecan, Switzerland) plate reader where measurements at OD625 (optical density at 625 nm) were recorded every 30 min. After 24 h, the lowest concentration of antimicrobial compound that inhibited growth was determined as the MIC.

Minimum Bactericidal Concentration (MBC) Assay. Following 24 h incubation of the 96-well flat-bottom plates at 37 °C, 3 μL of the culture from each well was pipetted out onto Modified Letheen Agar (Becton Dickinson) with 1.5% of Tween 80 (Sigma-Aldrich, MA, USA) (MLAT) agar plates. The plates were incubated at 37 °C for 24 h. The lowest concentration of antimicrobial compound with no growth was determined as the MBC.

S. aureus Membrane Staining and Immobilization. *Staphylococcus aureus* (*S. aureus*) was chosen as the bacterial model in this study as they are the most commonly found bacteria on human skin. *S. aureus* was labeled with lipophilic Nile Red dye (ThermoFisher Scientific, MA, USA) (2 μM) in culture solution (OD 1.5 at 600 nm). The sample was incubated in the dark for 20 min at room temperature, followed by centrifugation at 4000 rpm for 10 min (3 times). The stained cells were resuspended with saline solution before being seeded on a plasma-cleaned MatTek dish (PDC-32G, Harrick Plasma, NY, USA). The sample was then equilibrated for 20 min and washed 5 times with normal saline solution. For TIRF imaging, saline solution was added into the chamber. Cells were then measured either in saline solution or in the presence of various concentrations of different compounds. The compounds tested in this work are (Table 1):

Table 1. Antimicrobial Compounds

compounds		MIC (ppm)
BAC	benzalkonium chloride	3.13
Kathon	methylisothiazolinone	125
EHG	ethylhexylglycerin	1000
CG	caprylyl glycol	2500
SA	sorbic acid	4000
PO	piroctone olamine	50

Benzalkonium chloride (Sigma-Aldrich, MA, USA), Methylisothiazolinone (Thor, Speyer, Germany), Ethylhexylglycerin (Ashland, DE, USA), Caprylyl Glycol (Symrise, Holzminden, Germany), Sorbic Acid (Celanses, TX, USA) and Piroctone Olamine (Clariant, Muttenz, Switzerland). The compounds were used without further purification and were dissolved in saline solution to 0.3−1.0 MIC of the respective compound.

ITIR Microscope Settings. Measurements we performed on an Olympus microscope (IX83) with a motorized TIRF illumination combiner (cellTIRF-4Line IX3-MITICO, Olympus, Tokyo, Japan), an oil-immersion objective (Apo N, 100, NA 1.49, Olympus) and a 561 nm laser (Cell, Olympus). We used a laser power of 2.06 mW after the objective. A ZT 405/488/561/640rpc (Chroma Technology Corp, VT, USA) dichroic mirror was used to reflect the lasers into the back focal plane of the objective, with the incidence angle adjusted by Olympus cellSens Imaging software v3.1.1 to achieve TIRF mode. After the objective and dichroic, the signal was filtered using a laser quad band ZET 405/488/561/647 m (Chroma Technology Corp) emission filter for TIRF applications and directed to the detector. As acquisition camera we used an EMCCD (DU860, Andor Technology, Belfast, UK) with a pixel size of 24 μm. The Point Spread Function (PSF) of the system, characterized by the $1/e^2$ radius, was measured by calibration with a known sample: 0.5 mM 1,2-dioleoyl-*sn*-glycero-3-phophocholine (DOPC) and 50 nM Rhodamine PE (14:0 Liss Rhod PE), both supplied by Avanti Polar Lipids (AL, USA) with a resulting value of 0.96 λ/NA.[19] The excitation and emission wavelengths for Nile Red are 552 and 636 nm, respectively.

Imaging Total Internal Reflection-Fluorescence Correlation Spectroscopy (ITIR-FCS) Measurements and Analysis. ITIR-FCS measurements were recorded at 100 × 100 pixels and 50,000 frames at 2 ms time resolution. The ImageJ v1.53q plugin Imaging_FCS v1.64[22] was used to correct photobleaching during acquisition with a polynomial of fourth order and calculate the temporal correlation functions with a (p, q) = (16, 10) correlator scheme.[18] The resulting ACFs were fitted with the following theoretical ACF:

https://doi.org/10.1021/acs.analchem.4c05698
Anal. Chem. 2025, 97, 9648−9654

$$G(\tau) = \frac{1}{N}\left(\frac{\mathrm{erf}(p(\tau)) + \frac{e^{-(p(\tau))^2}-1}{\sqrt{\pi}p(\tau)}}{\mathrm{erf}\left(\frac{a}{\omega_0}\right) + \frac{\omega_0}{a\sqrt{\pi}}\left(e^{-\frac{a^2}{\omega_0^2}} - 1\right)} + G_\infty\right)^2 \quad (1)$$

$$p(\tau) = \frac{a}{\sqrt{4D\tau + {\omega_0}^2}}$$

Here, a denotes the size of a single square pixel on the CCD chip, in our case 240 nm (24 μm divided by the magnification of 100x), and ω_0 represents the radius of the Gaussian approximation of the microscope's point spread function. ω_0 is determined according to the protocol by Bag et al.[19] G_∞ corresponds to the ACF's convergence value at long correlation times, which is theoretically 0. The parameters N, D, and G_∞ are fitted, and the goodness-of-fit is evaluated using the χ^2 value.

Image Processing. Bright Field (BF) images (Figure 2A) were smoothened with a 3-pixel radius circular averaging filter. An adaptive threshold was calculated as 110% of the average intensity of the smoothed image. The original BF images were binarized with this threshold, followed with cleaning steps (Figure S1, Supporting Information). All the objects from the binary mask were classified into different categories, such as individual cells, clustered cells and noise objects, based on area, circularity, and aspect ratio (Figure S1, Supporting Information). Image processing was implemented in MATLAB R2019b (The MathWorks, Natick, MA, USA). Only data of pixels on the segmented bacteria were then analyzed by FCS. The correlation functions were fitted and the average number of particles in a pixel, N, and the diffusion coefficient, D, were automatically extracted (Figures S1 and S2). Only pixels with physiologically realistic D values ($0.01 < D < 10$ $\mu m^2/s$), had amplitudes above the noise background ($N < 1200$), and had an acceptable quality of fit ($\chi^2 < 1.2$) were retained (see Figure S2). To avoid that single cells are overrepresented in the analysis, we selected then the ACF with the highest amplitude as the in-focus point of the cell for analysis (for a comparison of the results for all valid ACFs vs only the optimal ACF per cell, see Figure S3).

Isothermal Microcalorimetry Measurement on Metabolic Activity. Plastic inserts from the CalWell (Symcel, Solna, Stockholm) were added individually into the titanium vials, which were loaded on a 48-well CalPlate (Symcel). The assay was conducted similarly to the MIC assay. Briefly, the wells were filled with 100 μL of TSB. An antimicrobial compound was added to the first well in each row to create two times the desired highest working concentration. Subsequently, a 2-fold serial dilution was carried out starting from the first well in each row. Overnight culture of *S. aureus* was adjusted to ~ 5 Log10 CFU/ml. A volume of 100 μL of the adjusted culture was added to each well. The vials were capped before loading the CalPlate into the calorimetric instrument. The heat produced is continuously captured and analyzed with the CalView software (Version 2020−10, Symcel).

Statistical Analysis. The results were expressed as the mean ± standard error of data obtained. To test any significant differences, Tukey's Honestly Significant Difference (HSD) test was performed using the JMP software for statistical analysis (Pro 16.1.0, JMP Statistical Discovery LLC).

RESULTS AND DISCUSSION

Membrane Fluidity of *S. aureus*. *S. aureus* cells, which are spherical in shape with a diameter of 0.5−1.5 μm (Figure 1A), were stained with Nile Red and subsequently immobilized on a coverslip (see Methods). We first recorded a bright field image as a reference point, before collecting TIRF stacks of 100 × 100 pixels and 50,000 frames at 2 ms time resolution. TIRF illumination ensures that only the first ~ 100 nm of the sample are collected and thus the surface-proximal membrane of the bacteria. In *S. aureus*, a Gram-positive bacterium, the envelope consists of an inner membrane and a thick peptidoglycan cell wall. Nile Red primarily integrates into the inner membrane of *S. aureus*; compared to partitions into both inner and outer membranes of Gram-negative bacteria. Since TIRF illumination penetrates beyond the 4−10 nm thickness of bacterial membranes, we cannot exclude some contribution from the inner membrane structures if the label is taken up into the cell. Nevertheless, changes in membrane fluidity due to antimicrobials are sensitively measured.

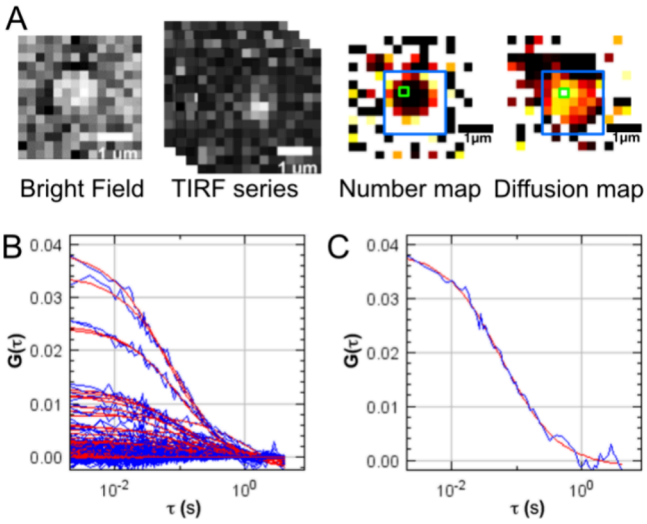

Figure 1. ITIR-FCS measurements on bacterial membranes. (A) ITIR image stack with 2 ms per frame is collected with a corresponding bright field image recorded as reference for cell location. Number maps (average number of particles per pixel) and Diffusion maps are derived from the autocorrelation analysis. (B) Autocorrelation functions measured within one single bacteria area (blue box in panel A). (C) The autocorrelation curve function at the in-focus point (green box in panel A) is considered representative and was used to determine the Nile Red diffusion coefficient in that particular cell.

Due to the spherical shape of *S. aureus* cells, only a tiny area of the bacterial membrane attached to the coverslip surface is in-focus. We therefore identified those pixels that are in focus by the maximum amplitude of the correlation functions, i.e. by the lowest values in the number map.[28] These pixels provide the most representative diffusion coefficient value for each bacteria cell (Figure 1B,C and Figure S4).

The typical diffusion coefficient of Nile Red in *S. aureus* membrane is 0.4−0.7 $\mu m^2/s$ and the distribution of Diffusion coefficients is shown in Figure 2C, consistent with earlier publications,[29−31] while the lipid diffusion on giant unilamellar vesicles lies between 6 and 12 $\mu m^2/s$ and 1−6 $\mu m^2/s$ for supported lipid bilayers.[32−34]

To automatically and efficiently extract and analyze data, we developed an image processing pipeline followed by statistical

https://doi.org/10.1021/acs.analchem.4c05698
Anal. Chem. 2025, 97, 9648−9654

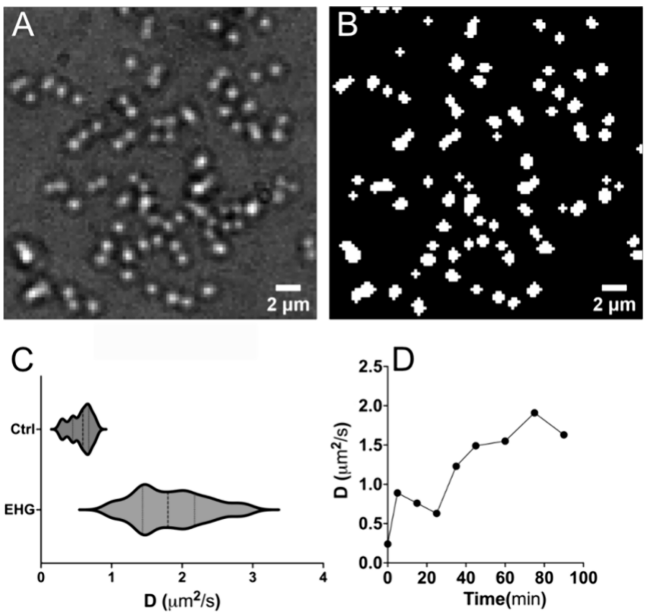

Figure 2. Image segmentation allows automatic data extraction and evaluation. (A) A bright field image of a field of view with around ∼ 80 bacterial cells. (B) Binary mask with attached cells identified and segmented. (C) Distributions of diffusion coefficients of the control group and EHG treated group (EHG treatment at 0.5MIC for 60 min). (D) Diffusion coefficient changes of a single cell treated with EHG at 0.5MIC over 90 min.

analysis (Figure 2 and Figure S1). This pipeline enables the assessment of diffusion coefficient distributions across cell populations (Figure 2C) while also allowing single-cell analysis to examine the compound's effects on any individual cell within the field of view (Figure 2D).

Effect of Subinhibitory Concentration Antimicrobial Compound Ethylhexylglycerin (EHG) on Lipid Membrane Dynamics of *S. aureus*. We examined the effect of antimicrobial compounds on membrane fluidity. The diffusion coefficient of untreated *S. aureus* cells served as control.

Ethylhexylglycerin (EHG), a glyceryl ether commonly used in cosmetics as a preservative, is diluted to four sub-MIC concentrations (0.3−1MIC with 1MIC = 1000 ppm for EHG) and incubated with *S. aureus* cells over 90 min. FCS measurements were acquired every 10 min. All measurements were acquired on the same cells.

The time course (Figure 3A) and dose response (Figure 3B) reveal that EHG treatments disturb bacterial membranes even at sub-MIC concentrations. EHG treatment resulted in significantly higher diffusion coefficients in dependence on concentrations and incubation time (up to 5-fold for 90 min treatment at 1 MIC) compared to untreated cells. FCS measurements on dead cells or cells with severely compromised membranes either failed to generate ACF profiles, or provided values considered as nonphysiological for N and D, and were filtered out. The population of dead/compromised cells is plotted in Figure 3C.

Since all measurements were collected on the same set of cells, we have the capability to track the status of each individual cell. The diffusion coefficient changes of one specific cell treated with EHG at 0.5 MIC concentration are shown in Figure 2D, and another sample treated with EHG at 1 MIC concentration is shown in Figure 3E. There is a clear left shift of its ACF profiles with incubation time (Figure 3F from dark

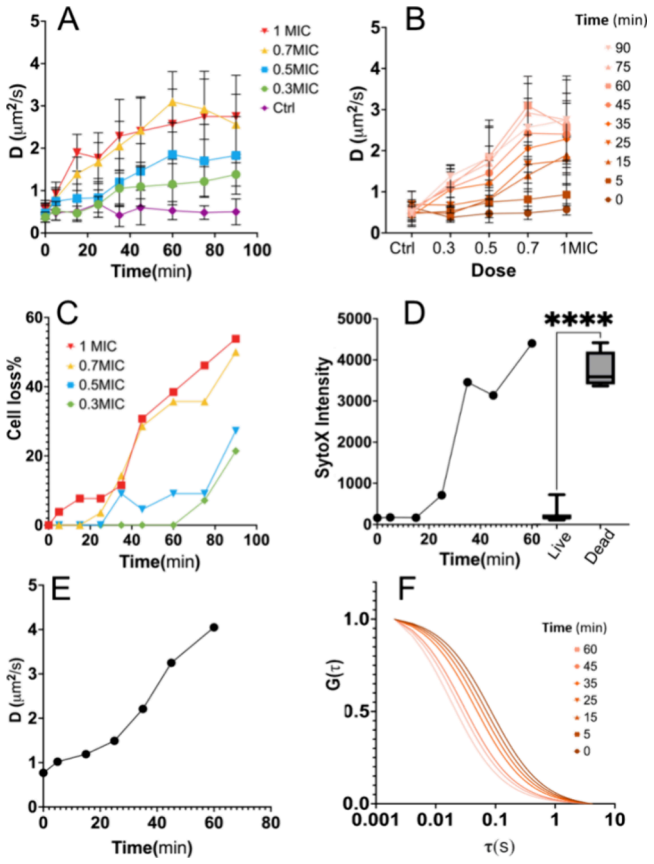

Figure 3. Influence of antimicrobial compound EHG on the membrane fluidity of bacteria and cross-validation with SytoX dye. (A) Time course curves of diffusion on bacterial membranes with EHG treated with sub-MIC concentrations. (B) Dose-response curves of diffusion on bacterial membranes with EHG treated over 90 min. (C) Corresponding percentage of cell loss with EHG treated cells with sub-MIC concentrations. (D) Change of SytoX intensity. (D insertion) Box-plots of SytoX Intensities of live cells and dead cells. (E) Diffusion coefficients of one *S. aureus* cell treated with EHG 1MIC for 60 min from the same sample. (F) Normalized ACF fits of the cell in E.

red to light pink). The narrower widths of the autocorrelation functions after EHG treatment indicate that the diffusion in the bacterial membrane is faster and thus the membrane is more fluid, an early indication of antimicrobial activity.

We examined cell viability with SytoX (ThermoFisher), which is a nucleic acid stain impermeable to live cells. The SytoX signal in *S. aureus* cells treated with EHG at 1 MIC increased as the cell membrane was gradually compromised with increasing incubation time (Figure 3D). Compared to the average SytoX signal of live and dead cells, the example cell sustained irrecoverable damage after treatment of 30 min, which is the earliest time an antimicrobial effect can be attested. Meanwhile, the diffusion coefficient immediately increased upon incubation with EHG and then continuously rose during treatment up to 60 min. This demonstrates that our method is much more sensitive to short-term changes in membrane fluidity induced by antimicrobial compounds, which increased from 0.57 ± 0.14 (SD) $\mu m^2/s$ before treatment to 0.93 ± 0.27 (SD) $\mu m^2/s$ within 5 min and 2.28 ± 0.87 (SD) $\mu m^2/s$ after 30 min treatment with EHG at 1 MIC.

https://doi.org/10.1021/acs.analchem.4c05698
Anal. Chem. 2025, 97, 9648−9654

Effect of Sub-MIC Antimicrobial Compounds on Lipid Membrane Dynamics of *S. aureus*. We extended the experiments to five more different compounds (Table 1) to demonstrate the possibility of imaging FCS for screening for antimicrobial activity in general and to examine the effective concentration range. The time course and dose response curves for these additional five compounds are shown in Figure 4 (data for EHG is described in the previous section and Figure 3). The results indicate that typically about 30 min of incubation is sufficient to obtain significant results. We observed a continuous increase of the average diffusion coefficient for cells treated with low concentrations compared to the MIC, whereas there usually are more fluctuations or variations in the time course curves of high concentration treatments close to the MIC, especially at late time points. At low concentrations, although the antimicrobial compounds lead to membrane changes, *S. aureus* cells survive. However, at high concentration treatments, we observe drastic changes in membrane diffusivity and cells gradually die with increasing treatment time. This is especially observed for cells with fast increasing D at early time points (Refer to Figure 3C and Figure S5). The loss of data from these cells results in an increase in the standard deviations of the time course curves.

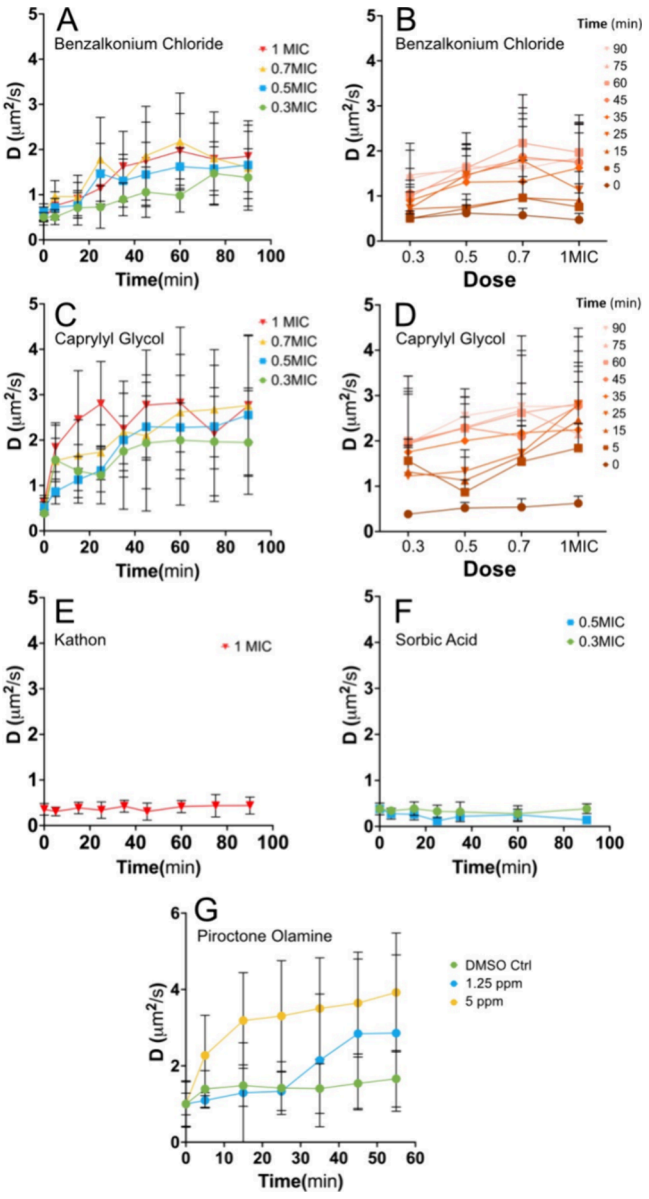

Figure 4. Influence of antimicrobial compounds on the membrane fluidity of bacteria. (A) Time course curves and (B) dose−response curves of diffusion on bacterial membranes with BAC treated with sub-MIC concentrations. (C) Time course curves and (D) dose−response curves of diffusion on bacterial membranes with CG treated at sub-MIC concentrations. Time course curves of diffusion on bacterial membranes with (E) Kathon, (F) SA and (G) PO treatment.

Among the six antimicrobial compounds, EHG, BAC, CG and PO induced a significant increase in membrane diffusion, while Kathon and SA had no effect on lipid diffusion of bacterial membranes. Using a BacLight live/dead dye kit (ThermoFisher) (Figure S6), we observed an increasing number of dead cells in Kathon and SA treated cells, which implies that these two compounds may employ antimicrobial mechanisms that do not target the bacterial membranes, and thus differ from the other four compounds.

Isothermal Microcalorimetry (IMC) Profiles of Antimicrobial Compounds. To cross-validate our results of compounds with different antimicrobial mechanisms, we performed isothermal microcalorimetry analysis of two representative preservative compounds, Kathon and BAC.

With the addition of Kathon CG to *S. aureus* at increasing concentrations, an increase in the time to peak (TTP) was observed (Figure 5A). The TTP for untreated *S. aureus*

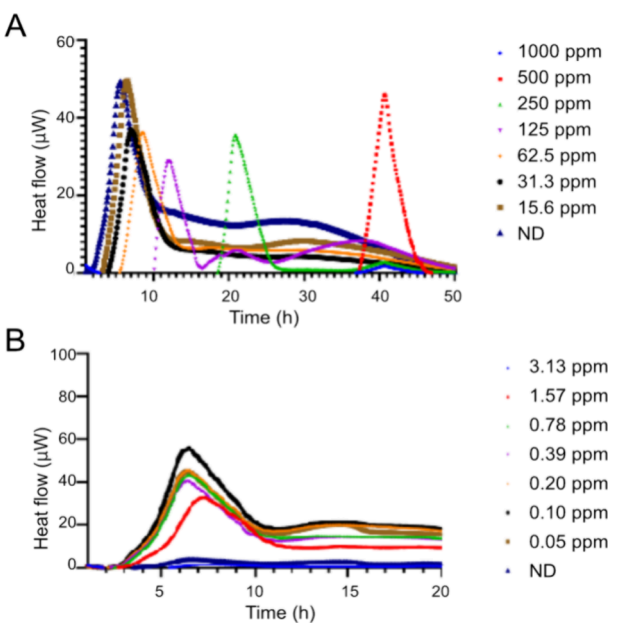

Figure 5. Isothermal microcalorimetry profiles of (A) Kathon CG and (B) BAC.

(Figure 5A) and *S. aureus* treated with 15.6 ppm Kathon CG were 3.32 ± 0.08 (SE) hours and 3.99 ± 0.19 (SE) hours. As the concentration of Kathon CG increased to 31.3 ppm, the corresponding TTP increased to 4.76 ± 0.35 (SE) hours. This increase was further demonstrated by the addition of 62.5, 125, and 250 ppm of Kathon CG, with a TTP of 6.38 ± 0.54 (SE) hours, 10.79 ± 1.56 (SE) hours, and 22.98 ± 1.55 (SE) hours, respectively. At 500 ppm and above, no heat flow was observed for *S. aureus*, indicating that the metabolism of *S. aureus* ceased at 500 ppm. Through student's *t* test performed on the TTP of

https://doi.org/10.1021/acs.analchem.4c05698
Anal. Chem. 2025, 97, 9648−9654

S. aureus in the presence of Kathon CG, the TTP with Kathon CG at concentrations of 250, 125, and 15.6 ppm were considered significantly different. While the TTP increased with increasing Kathon CG concentration, no significant difference was observed for the maximum heat flow (MHF), indicating that *S. aureus* was growing to saturation (Figure 5A).

This heat flow profile (increase in TTP with similar MHF) could be indicative of the inhibitory MoA of Kathon CG, which delays cell growth and metabolism. This was further supported by the growth curves (recorded every 30 min for 24 h), where the lag phase of *S. aureus* increased as the concentration of Kathon CG increased. At 31.3 ppm of Kathon CG, the lag phase was 6.58 ± 0.57 (SE) hours, compared to 8.83 ± 0.75 (SE) hours when the concentration of Kathon CG was 62.5 ppm. Like the heat flow profile, the growth curves of *S. aureus* indicated that growth to saturation was observed at all concentrations of Kathon CG, signifying that *S. aureus* growth was only inhibited.

On the contrary, BAC is a known membrane disruptor.[35] In the heat flow profiles obtained in the presence of Kathon CG, a gradual difference was observed in the TTP or the MHF, respectively, as the concentration of the compound increased. In the case of BAC, no significant difference in the TTP was observed between 0.05−0.78 ppm of BAC (Figure 5B). The MHF was also similar between 0.05−0.78 ppm as all concentrations were not significantly different from 0.05 ppm of BAC from the student's *t* test. This could be attributed to its membrane disruption MoA, which leads to immediate bactericidal effects. These results were also reflected in the growth curves. At nonbactericidal concentrations between 0.05−0.78 ppm, full growth of *S. aureus* was observed, similar to the untreated cells (dark purple), while no growth was observed at 3.13 ppm BAC.

Despite the student's *t* test identifying a significant difference in the heat flow profile when *S. aureus* was subjected to 1.57 ppm, obtaining a TTP and MHF at 1.57 ppm were 4.36 ± 0.43 (SE) hours and 39.94 ± 3.50 (SE) μW, respectively, no clear trend was observed at the lower concentrations applied. This signifies that the slight increase in the TTP could be due to the high concentration of the compound, close to the MBC value. In contrast to the untreated *S. aureus*, the TTP and MHF were 3.32 ± 0.08 (SE) hours and 43.5 ± 1.14 (SE) μW, respectively.

CONCLUSIONS

This work describes a new screening tool for antimicrobials with ITIR-FCS, which provides a more sensitive, rapid and quantitative response to the subtle disruption of bacterial membrane dynamics induced by membrane-active antimicrobial compounds at sub-MIC concentrations. The approach was supported by a screening assay of six antimicrobial compounds with different mechanisms, and was cross-validated with traditional cell viability assays and isothermal microcalorimetry. This new approach detects changes of membrane dynamics upon antimicrobial challenge within less than 30 min and generates dose−response curves within 1−2 h, speeding up the screening process compared to the 6−24 h' time span of traditional screening tools. The ITIR-FCS assay can be easily adapted to other microbial screens and when conducted in microchannels can be multiplexed, contributing to ongoing efforts to enhance the efficacy of new generation membrane-active preservatives and antibacterial compounds.

ASSOCIATED CONTENT

Supporting Information

The Supporting Information is available free of charge at https://pubs.acs.org/doi/10.1021/acs.analchem.4c05698.

Figure S1 describes the image processing steps for bacterial cell identification; Figure S2 shows selected ACF examples for ACF evaluation; Figure S3 shows a comparison of the diffusion coefficient distributions for valid ACFs and optimal ACFs; Figure S4 shows the consistency of N map and D maps; Figure S5 shows the percentage of cell loss with antimicrobial treatment over 90 min; Figure S6 shows the results of BacLight LIVE/DEAD bacterial viability test with SA treatment (PDF)

AUTHOR INFORMATION

Corresponding Author

Thorsten Wohland − *Centre for BioImaging Sciences, National University of Singapore, Singapore 117557, Singapore; Department of Chemistry, National University of Singapore, Singapore 117543, Singapore; Department of Biological Sciences, National University of Singapore, Singapore 117558, Singapore*; Email: twohland@nus.edu.sg

Authors

Shiwen Zhu − *Centre for BioImaging Sciences, National University of Singapore, Singapore 117557, Singapore; Department of Biological Sciences, National University of Singapore, Singapore 117558, Singapore*; orcid.org/0009-0000-2566-7715

Yu Wang − *Beauty Revealed, Procter & Gamble International Operations SA Singapore Branch, Singapore 138547, Singapore*; orcid.org/0000-0003-0506-2932

Shi Min Sherilyn Chong − *Beauty Revealed, Procter & Gamble International Operations SA Singapore Branch, Singapore 138547, Singapore*

Complete contact information is available at: https://pubs.acs.org/10.1021/acs.analchem.4c05698

Author Contributions

Y.W. and T.W. conceived the study. S.Z. and Y.W. performed the ITIR-FCS experiments and data evaluation. S.Z. wrote the segmentation algorithm. S.M.S.C. performed the isothermal microcalorimetry assay. All authors contributed to the article writing.

Notes

The authors declare no competing financial interest.

ACKNOWLEDGMENTS

The project was funded by a P&G and A*STAR joint research grant.

REFERENCES

(1) Pastor-Nieto, M. A.; Alcántara-Nicolás, F.; Melgar-Molero, V.; Pérez-Mesonero, R.; Vergara-Sánchez, A.; Martín-Fuentes, A.; González-Muñoz, P.; de Eusebio-Murillo, E. *Actas Dermo-Sifiliogr.* **2017**, *108*, 758−770.

(2) Halla, N.; Fernandes, I. P.; Heleno, S. A.; Costa, P.; Boucherit-Otmani, Z.; Boucherit, K.; Rodrigues, A. E.; Ferreira, I. C. F. R.; Barreiro, M. F. *Molecules* **2018**, *23*, 1571.

(3) Mingeot-Leclercq, M.-P.; Décout, J.-L. *MedChemComm* **2016**, *7* (4), 586−611.

(4) Hurdle, J. G.; O'Neill, A. J.; Chopra, I.; Lee, R. E. *Nat. Rev. Microbiol* **2011**, *9* (1), 62−75.
(5) Teixeira, V.; Feio, M. J.; Bastos, M. *Prog. Lipid Res.* **2012**, *51* (2), 149−177.
(6) Fjell, C. D.; Hiss, J. A.; Hancock, R. E.; Schneider, G. *Nat. Rev. Drug Discov* **2012**, *11* (1), 37−51.
(7) Epand, R. M.; Vogel, H. J. *Biochimica et Biophysica Acta (BBA)-Biomembranes* **1999**, *1462* (1−2), 11−28.
(8) Niu, L.; Wohland, T.; Knoll, W.; Köper, I. *Biointerphases* **2017**, *12* (4), No. 04E404.
(9) Ritchie, K.; Spector, J. *Biopolymers* **2007**, *87* (2−3), 95−101.
(10) Ilangumaran Ponmalar, I.; Swain, J.; Basu, J. K. *Biomater Sci.* **2022**, *10* (10), 2609−2617.
(11) Chow, D.; Guo, L.; Gai, F.; Goulian, M. *PLoS One* **2012**, *7* (10), No. e48600.
(12) Mahler, L.; Wink, K.; Beulig, R. J.; Scherlach, K.; Tovar, M.; Zang, E.; Martin, K.; Hertweck, C.; Belder, D.; Roth, M. *Sci. Rep.* **2018**, *8* (1), 13087.
(13) Kaminski, T. S.; Scheler, O.; Garstecki, P. *Lab Chip* **2016**, *16* (12), 2168−2187.
(14) Schug, K. A.; Wang, E.; Shen, S.; Rao, S.; Smith, S. M.; Hunt, L.; Mydlarz, L. D. *Analytica chimica acta* **2012**, *713*, 103−110.
(15) Kim, T. K.; Hewavitharana, A. K.; Shaw, P. N.; Fuerst, J. A. *Applied and environmental microbiology* **2006**, *72* (3), 2118−2125.
(16) Kannan, B.; Har, J. Y.; Liu, P.; Maruyama, I.; Ding, J. L.; Wohland, T. *Analytical chemistry* **2006**, *78* (10), 3444−3451.
(17) Singh, A. P.; Krieger, J. W.; Buchholz, J.; Charbon, E.; Langowski, J.; Wohland, T. *Opt. Express* **2013**, *21* (7), 8652−8668.
(18) Wohland, T.; Maiti, S.; Macháň, R. *An introduction to fluorescence correlation spectroscopy*. IOP Publishing Ltd., 2020.
(19) Bag, N.; Sankaran, J.; Paul, A.; Kraut, R. S.; Wohland, T. *ChemPhysChem* **2012**, *13* (11), 2784−2794.
(20) Sankaran, J.; Bag, N.; Kraut, R. S.; Wohland, T. *Analytical chemistry* **2013**, *85* (8), 3948−3954.
(21) Sankaran, J.; Manna, M.; Guo, L.; Kraut, R.; Wohland, T. *Biophysical journal* **2009**, *97* (9), 2630−2639.
(22) Sankaran, J.; Shi, X.; Ho, L. Y.; Stelzer, E. H.; Wohland, T. *Opt. Express* **2010**, *18* (25), 25468−25481.
(23) Wohland, T.; Shi, X.; Sankaran, J.; Stelzer, E. H. K. *Opt. Express* **2010**, *18* (10), 10627−10641.
(24) Wadsö, L. *J. Therm. Anal. Calorim.* **2001**, *64* (1), 75−84.
(25) Wadsö, I. *Thermochimica acta* **2002**, *394* (1−2), 305−311.
(26) Tellapragada, C.; Hasan, B.; Antonelli, A.; Maruri, A.; de Vogel, C.; Gijon, D.; Coppi, M.; Verbon, A.; van Wamel, W.; Rossolini, G. M.; Canton, R.; Giske, C. G. *Clin. Microbiol. Infect.* **2020**, *26* (10), 1413.e1−1413.e7.
(27) von Ah, U.; Wirz, D.; Daniels, A. *BMC Microbiol.* **2009**, *9* (1), 106.
(28) Aik, D. Y.; Wohland, T. *Biophys. J.* **2022**, *121* (14), 2663−2670.
(29) van den Wildenberg, S. M.; Bollen, Y. J.; Peterman, E. J. *Biopolymers* **2011**, *95* (5), 312−21.
(30) Barbotin, A.; Billaudeau, C.; Sezgin, E.; Carballido-López, R. *Biophys. J.* **2024**, *123* (16), 2484−2495.
(31) Leptihn, S.; Har, J. Y.; Chen, J.; Ho, B.; Wohland, T.; Ding, J. L. *BMC Biol.* **2009**, *7*, 22.
(32) Ng, X. W.; Teh, C.; Korzh, V.; Wohland, T. *Biophys. J.* **2016**, *111* (2), 418−429.
(33) Machan, R.; Hof, M. *Biochim. Biophys. Acta* **2010**, *1798* (7), 1377−91.
(34) Guo, L.; Har, J. Y.; Sankaran, J.; Hong, Y.; Kannan, B.; Wohland, T. *ChemPhysChem* **2008**, *9* (5), 721−8.
(35) Merchel Piovesan Pereira, B.; Tagkopoulos, I.; Vieille, C. *Appl. Environ. Microbiol.* **2019**, *85* (13), No. e00377-19.

https://doi.org/10.1021/acs.analchem.4c05698
Anal. Chem. 2025, 97, 9648−9654